Published in final edited form as:
J Control Release. 2012 August 20; 162(1): 233–241. doi:10.1016/j.jconrel.2012.06.028.

Fabrication of Magnetic Nanoparticles with Controllable Drug Loading and Release through a Simple Assembly Approach

Chen Fang[a], **Forrest M. Kievit**[a], **Omid Veiseh**[a], **Zachary R. Stephen**[a], **Tingzhong Wang**[d], **Donghoon Lee**[b], **Richard G. Ellenbogen**[c], and **Mciqin Zhang**[*,a,b,c]

[a]Departments of Materials Science and Engineering, University of Washington, Seattle, Washington, 98195, USA

[b]Department of Radiology, University of Washington, Seattle, Washington, 98195, USA

[c]Department of Neurological Surgery, University of Washington, Seattle, Washington, 98195, USA

[d]Department of Neurological Surgery, The Fourth Affiliated Hospital of China Medical University, Shenyang, Liaoning, 110032, P.R. China

Abstract

Nanoparticle-based cancer therapeutics promises to improve drug delivery safety and efficacy. However, fabrication of consistent theranostic nanoparticles with high and controllable drug loading remains a challenge, primarily due to the cumbersome, multi-step synthesis processes conventionally applied. Here, we present a simple and highly controllable method for assembly of theranostic nanoparticles, which may greatly reduce batch-to-batch variation. The major components of this nanoparticle system include a superparamagnetic iron oxide nanoparticle (SPION), a biodegradable and pH-sensitive poly (beta-amino ester) (PBAE) copolymer, a chemotherapeutic agent doxorubicin (DOX). Here the polymer pre-loaded with drug is directly assembled to the surface of SPIONs forming a drug loaded nanoparticle (NP-DOX). NP-DOX demonstrated a high drug loading efficiency of 679 μg DOX per mg iron, sustained stability in cell culture media up to 7 days, and a strong r_2 relaxivity of 146 $mM^{-1} \bullet s^{-1}$ for magnetic resonance imaging (MRI). The drug release analysis of NP-DOX showed fast DOX release at pH 5.5 and 6.4 (as in endosomal environment) and slow release at pH 7.4 (physiological condition), demonstrating pH-sensitive drug release kinetics. *In vitro* evaluation of NP-DOX efficacy using drug-resistant C6 glioma cells showed a 300% increase in cellular internalization at 24 h post-treatment and 65% reduction of IC50 at 72 h post-treatment when compared to free DOX. These nanoparticles could serve as a foundation for building smart theranostic formulations for sensitive detection through MRI and effective treatment of cancer by controlled drug release.

Keywords

Drug Delivery; Magnetic Resonance Imaging; Nanoparticles; Theranostics

[*]CORRESPONDING AUTHOR ADDRESS: 302L Roberts Hall, Department of Materials Science and Engineering, University of Washington, Seattle, Washington, 98195, USA. Tel: (206) 616-9356. Fax: (206) 543-3100. mzhang@u.washington.edu.

1.Introduction

Cancer remains one of the most devastating diseases despite continuous development and innovation in cancer therapy. Of the current treatment options, chemotherapy remains a major component of cancer therapeutic regimens [1]. However, the efficacy of chemotherapy is impaired by the development of the multidrug resistance (MDR) phenotype by cancer cells. MDR is characterized by the overexpression of ATP-binding cassette (ABC) transporters which increase the efflux of chemotherapeutic drugs out of cancer cells before the drug can reach its intracellular site of action [2]. MDR inhibitors have been developed to improve the drug accumulation in cancer cells, but their widespread clinical use has been limited by high toxicity and low efficacy [2].

Nanoparticle-based therapeutics offers a new approach to circumvent MDR by improving the intracellular accumulation of chemotherapy drug [3, 4]. Further, the therapeutic nanoparticles harnessed with imaging components can produce nanotheranostic (diagnosis + therapy) systems that enable non-invasive, real-time monitoring of drug delivery and therapeutic response [5, 6]. The combination of imaging and therapeutic functions in a single entity helps develop highly customizable therapies that eventually could lead to the realization of personalized medicine [7, 8]. Of the theranostic nanoparticles being studied, superparamagnetic iron oxide nanoparticles (SPIONs) are appealing owing to their intrinsic superparamagnetism that provides contrast in magnetic resonance imaging (MRI) [9–11], and solid core to which therapeutics can be easily arranged [12–15]. Furthermore, iron oxide has been known to be biocompatible and biodegradable [16–20] and a number of drug loaded theranostic SPIONs have been investigated [21–29].

Despite the promise of these theranostic nanoparticles, fabrication of reproducible and consistent formulations with controlled drug loading and release profiles remains a significant challenge and a major barrier to their clinical application. The difficulty lies in fabrication schemes that involve complex, multi-step synthesis procedures that can multiply and accumulate the variations or fluctuations from each step leading to significant batch-to-batch inconsistencies and inefficient drug loading [30].

To address these challenges, we developed a simple and highly reproducible approach to fabricate theranostic nanoparticles that can provide efficient drug loading, controllable drug release, and imaging capability. The major components of this theranostic nanoparticle formulation include a biodegradable and pH-sensitive poly (beta-amino ester) (PBAE) copolymer, the chemotherapeutic agent doxorubicin (DOX), and a SPION core. PBAE is a class of polymers containing both pH-responsive tertiary amines and biodegradable ester groups along the backbone, and has been evaluated as a vehicle for gene [31–33] and drug [34, 35] delivery. DOX has been thoroughly investigated [36] and received regulatory approval for the treatment of a variety of solid tumors and hematological cancers [37]. Unlike conventional methods by which multiple coating components are individually assembled onto nanoparticles through multiple reaction steps and thus the control of the component ratios and optimization of drug loading is difficult, we directly assemble multiple components including DOX, dopamine (DA) for anchoring on iron oxide surfaces, and poly (ethylene glycol) (PEG) for improving aqueous stability and reducing protein fouling onto PBAE backbone [16, 19, 20]. The PBAE polymer system was then assembled on SPIONs using a highly efficient and controllable chemical scheme to produce DOX-loaded nanoparticles (NP-DOX).

NP-DOX and free DOX were applied to a drug-resistant C6 cell line (C6-ADR) [22] to evaluate the feasibility of NP-DOX for overcoming MDR. The DOX dose required for NP-DOX or free DOX to reduce cell viability by 50% (IC50) was determined by the Alamar

Blue cell viability assay. The cellular internalization of nanoparticles was evaluated by iron quantification (Ferrozine assay), DOX quantification, as well as fluorescent microscopy.

2. Experimental Section

2.1. Materials

Doxorubicin•HCl (DOX), dopamine•HCl (DA), O,O'-bis(3-aminopropyl) diethylene glycol (BADG), di(ethylene glycol) diacrylate (DEGDA) and all general chemicals were purchased from Sigma-Aldrich (St. Louis, MO) unless otherwise specified. Methoxy-poly(ethylene glycol)-amine (mPEG-NH_2, MW 2,000) was purchased from Laysan Bio (Arab, AL). Dulbecco's modified Eagle media (DMEM), antibiotic-antimycotic (AA), WGA-AF488, Prolong Gold anti-fade reagent with DAPI and agarose gel were purchased from Invitrogen (Carlsbad, CA). Fetal bovine serum (FBS) was purchased from Atlanta Biologicals (Lawrenceville, GA).

2.2. Synthesis of PBAE polymers

(1) DOX-loaded polymer (PBAE-DOX)—Molar ratio of monomers was set at 50:19:19:12 (DEGDA:PEG:DA:DOX). To a 25 mL flask, 9 mg doxorubicin, 11.0 mg DEGDA, 32.8 mg mPEG-NH_2 and 7.8 mg DA were added. 5 μL triethylamine dissolved in 1 mL DMSO were added to the flask, and the flask was sealed and purged with nitrogen. The reaction proceeded at 50°C for 44 h. Excess amount (11 mg) of BADG was added to the flask to terminate the polymerization process. The reaction continued for 4 h and the product was precipitated by the organic solvent ether and dissolved in 2 mL of water. To remove any unreacted reactants, aqueous solution of PBAE-DOX was passed through a PD-10 column packed with Sephadex G-25 resin. The eluate was lyophilized to yield a final product as a dark red solid.

(2) Control polymer (without DOX)—To evaluate the intrinsic toxicity of nanoparticles without DOX, polymer with no DOX loading (PBAE-C) was prepared in a similar way to PBAE-DOX at a molar ratio of 50:25:25:0 (DEGDA:PEG:DA:DOX).

2.3. Synthesis of PBAE-DOX-coated iron oxide nanoparticles

Oleic acid capped iron oxide nanoparticles (core size: 12 nm) were synthesized according to a published procedure [38]. The iron concentration of nanoparticles was determined by ICP-AES. The PBAE-DOX was coated to nanoparticle surface via ligand exchange reaction. 20 mg of PBAE polymer were dissolved in 200 μL of DMSO and mixed with 1.8 mL of THF containing 2 mg nanoparticles. The mixture was placed in a flask, sealed and purged with nitrogen. The mixture was allowed to react for 24 h at room temperature in dark. Nanoparticles were precipitated by ether and then redispersed in DMSO for long-term storage. Before experiments, nanoparticles were precipitated again by ether and then redispersed in D.I water. Centrifugal filters were used to remove any unbound polymer and residual organic solvents. The concentrated nanoparticles were diluted with D.I. water to 100 μg/mL equivalent concentration of drug.

2.4. Nanoparticle characterizations

The size and zeta potential of nanoparticles were measured by dynamic light scattering (DLS) using a DTS Zetasizer Nano (Malvern Instruments, Worcestershire, UK). Nanoparticles concentrations were 100 μg/mL for all measurements. Nanoparticle stability was determined in DMEM containing 10% FBS and 1% AA.

Drug loading was determined by the average of DOX content of three independent batches of polymers or NPs. The absorbance of polymer or dissolved NPs solutions were recorded by a UV-vis spectrometer (Agilent Technologies, Santa Clara, CA). The wavelength of UV absorption for DOX was 494 nm. Fluorescence measurements were conducted with a SpectraMax M2 microplate reader (Molecular Devices, Union City, CA) using excitation and emission wavelengths of 485 nm and 590 nm, respectively, for DOX.

Samples for ^{1}H-NMR analysis were prepared by dissolving 50 μg of nanoparticles in 50 μL of DCl and then diluted with 950 μL of D_2O. NMR spectra were acquired by a Avance 300 spectrometer (Bruker Corporation, Billerica, MA) operating at 300 MHz (^{1}H) and 298 K, with number of scans = 128, acquisition time = 1 s, relaxation delay (D1) = 7 s.

For the measurement of the drug release profile, nanoparticle samples were loaded in dialysis devices (Slide-A-Lyzer MINI dialysis unit, 100 μL capacity, 2,000 MWCO, Pierce Biotechnology, Rockford, IL), and dialyzed against 10 mL PBS buffer at pH 7.4, 6.4 or 5.5. Aliquots of samples were taken at 4 h, 24 h, 48 h, 60 h and 72 h. The fluorescence measurement was conducted using a microplate reader set to the same parameters described above.

2.5. Cell culture

Rat glioma C6 cells were purchased from American Type Culture Collection (ATCC, Manassas, VA) and maintained in DMEM containing 10% FBS and 1% antibiotic-antimycotic. DOX-resistant C6 cells (C6-ADR) were prepared from rat glioma C6 cells as described in a previous study [22]. C6-ADR cells were then frozen and stored in liquid nitrogen. Fresh aliquots of C6-ADR were used for experiments to ensure that C6-ADR did not lose their drug resistance.

2.6. Dose-response experiment

C6-ADR cells were plated at 10,000 cells per well in 96-well plates the night before treatment. Cells were then treated with free DOX or NP-DOX at 0, 10, 50, 100, 1000, and 10000 ng/mL DOX in 150 μL fully supplemented DMEM for 4 hrs before washing three times with PBS and adding 150 μL fresh fully supplemented DMEM. Cell viability was determined at 24, 48, and 72 hrs post-treatment using the Alamar Blue viability assay following the manufacturer's protocol. IC50 values were calculated from dose-response curves generated with a polynomial dose-response approximation using the Origin software package (OriginLab Corporation, Northampton, MA).

2.7. Quantification of cellular internalization of nanoparticles and DOX

Sensitive C6 and C6-ADR cells were plated at 100,000 cells per well in 24-well plates the night before treatment. Cells were then treated with 1000 ng/mL free DOX or equimolar concentration of DOX on NPDOX in 1 mL fully supplemented DMEM for 4 hrs before cells were washed three times with PBS and 1 mL fresh fully supplemented media added. The cell number per well was assessed using the Alamar Blue and calculated based on a previously prepared standard curve. At 4 hr and 24 hr time points, cells were solubilized with 100 μL concentrated HCl and further diluted with 400 μL of D.I. water. The concentration of intracellular iron was determined by the colorimetric Ferrozine iron quantification assay with modifications. To 300 μL of cell lysate, 200 μL of 4M NaOH, 400 μL of D.I. water and 90 μL of Ferrozine solution were added. The solution was vortexed, transferred to 96-well plates, and the absorbance of 562 nm was recorded. The iron concentration per cell was calculated based on a standard curve of iron and cell number from Bradford protein assay. At the same time, the concentration of DOX was determined by

fluorimetric measurement with a microplate reader, using excitation and emission wavelengths of 485 nm and 590 nm, respectively.

2.8. Fluorescence imaging

C6-ADR cells were plated at 500,000 cells per well in 6-well plates containing 22 × 22 mm glass cover slips the night before treatment. Cells were treated with 1000 ng/mL free DOX or NP-DOX with equimolar concentration of DOX in 2 mL fully supplemented DMEM for 4 hrs before cells were washed three times with PBS and 2 mL fresh fully supplemented media added. After 24 hrs, cells were washed three times with PBS, and fixed in 4 % formaldehyde (Polysciences Inc., Warrington, PA) for 30 min. Cell membranes were stained with wheat germ agglutinin, Alexa Fluor 488 conjugates (WGA-AF488, Invitrogen, Carlsbad, CA) following the manufacturer's protocol. The cover slips were then mounted on microscope slides using Prolong Gold anti-fade solution (Invitrogen, Carlsbad, CA) containing DAPI for cell nuclei staining. Images were acquired on an inverted fluorescent microscope (Nikon Instruments, Melville, NY) with the appropriate filters using a Nikon Ri1 Color Cooled Camera System and 60× oil objective Lens. For internalization pathway experiment, cells were treated with DOX or NP-DOX in the presence of 0.25 mM calcein for 4 hrs. Cell membranes were stained with WGA-AF647 conjugate. DOX and calcein uptake were analyzed using confocal microscopy (Zeiss 510 Meta).

2.9. MR imaging

T_2 relaxation measurements were performed on a 4.7-T Bruker magnet equipped with Varian Inova spectrometer (Varian, Inc., Palo Alto, CA). Samples of NP-DOX were suspended in 1% agarose at concentrations of 0, 0.0625, 1.25, 2.5, and 5 μg Fe/ml. A 5 cm volume coil and a spin-echo imaging sequence were used to acquire T_2-weighted images. Images were acquired using a repetition time (TR) of 3000 ms and echo times (TE) of 13.6, 20.0, 40.0, 60.0, 80.0 and 120.0 ms. The spatial resolution parameters were: acquisition matrix of 256 × 128, field-of-view of 35 × 35 mm, section thickness of 1 mm and two averages. The T_2 maps were generated by NIH ImageJ (Bethesda, MD) based on the equation, $SI = A \cdot \exp(-TE/T_2) + B$, where SI is the signal intensity, TE is the echo time, A is the amplitude, and B is the offset. R_2 maps were generated by taking the reciprocal of T_2 maps.

2.10. Statistical analysis

All experiments were run in triplicate and acquired data were expressed as mean ± standard deviation. Statistical significance was determined using Student's *t*-test. Values of * $P < 0.05$, ** $P < 0.01$, and *** $P < 0.001$ were considered significant.

3. Results

3.1. Synthesis and characterization of PBAE-DOX and PBAE- polymer

The synthesis scheme used to prepare PBAE-DOX and PBAE polymer is shown in Fig. 1. PBAE is synthesized through a reaction between bifunctional amines and diacrylate monomers (Fig. 1a). This Michael addition reaction results in covalent linkages between alkene groups of diacrylate and nitrogen atoms on bifunctional amine compounds. The reaction produces tertiary amine groups and ester linkages along the backbone of PBAE. The copolymer contains four basic units: DEGDA as the backbone unit, DA as the metal binding unit, PEG as the hydrophilic unit, and DOX as the anticancer drug unit (Fig. 1b). The yield of polymerization is 60.4%.

PBAE-DOX was characterized by ^{1}H-NMR spectroscopy (Fig. 2, upper panel). The distinct PEG peak at $\delta = 3.65$ ppm was clearly resolved, while the peak at $\delta = 6.7$ was associated

with the anthracycline ring of DOX. The peak at δ = 6.5 was assigned to the phenyl ring of DA. Peaks at δ = 2.5–2.8 ppm were associated with ethylene groups on the PBAE backbone. The weight ratios of PEG, DOX, and DA in PBAE (Fig. 3a) were determined by integration of the associated areas under ^{1}H-NMR spectrum curve (Fig. 2). Here, the feeding and loading ratios refer to the polymer component weight ratios before and after polymerization, respectively. PBAE-DOX was also characterized by UV-vis and fluorescence spectroscopy (Fig. 3b) to ensure preservation of DOX fluorescence properties and to further confirm and quantify the DOX loading. Free DOX emits red fluorescence at 590 nm and the spectrum shown in Fig. 3b confirms that PBAE-DOX conserved the fluorescent property of DOX with the absorbance maxima at 485 nm and emission maxima at 590 nm. The fluorescent property of PBAE-DOX was utilized in subsequent cellular imaging to reveal the intracellular distribution of NP-DOX. Using the absorbance measured from PBAE-DOX, we quantified that the weight of DOX accounts for 9.5% of the total PBAE weight (Table 1).

3.2. Synthesis and characterization of doxorubicin-loaded nanoparticles (NP-DOX)

The NP-DOX conjugate is formed through a ligand exchange reaction, where the oleic acid molecules on the surface of NP-OA are replaced by PBAE-DOX molecules (Fig. 1c). The DA units of PBAE-DOX contain catechol (ortho-benzenediol) groups, which form strong and stable bonds with metal oxide surfaces [25]. The ligand exchange process is performed in organic solvents under a nitrogen atmosphere to prevent oxidation of the dopamine unit. Success of the ligand exchange reaction in synthesis of NP-DOX was confirmed by ^{1}H-NMR spectra of dissolved NP-DOX (Fig. 2, lower panel). NMR spectra clearly resolved the characteristic PEG ethylene peak at δ = 3.65 ppm, consistent with PEG peak in the PBAE-DOX copolymer. Peaks associated with DOX and dopamine were not resolved in the spectra due to low sample concentration which is required to reduce peak broadening caused by iron in solution. DOX loading of NP-DOX was found to be 679 μg/mg iron (Table 2), in which the DOX amount is quantified by UV-vis and the amount of oxide is quantified by inductively coupled plasma-atomic emission spectroscopy (ICP-AES) following the method reported previously [39]. Quantification of DOX concentration prior to and after attaching to NPs using UV showed that the efficiency of DOX loading via ligand exchange process was about 90%.

TEM images (Fig. 4a) showed that the nanoparticles were highly dispersed before the ligand exchange process (NP-OA) and remained well dispersed and free of aggregation after ligand exchange (NP-DOX). Light scattering measurements indicated that the hydrodynamic size of NP-DOX in DMEM/10% FBS was ~80 nm initially, and no significant changes in size, visible cloudiness or precipitates were observed for up to a week (Fig. 4b), indicating the NPs retained good stability. The zeta of NP-DOX at pH 7.4 was −0.3 mV, close to neutral (Table 2).

To determine the kinetics of drug release from NP-DOX, the nanoparticles were incubated in aqueous buffers to induce the degradation of PBAE polymers and liberation of drug. The drug release experiments were performed at pH 5.5, pH 6.4, and pH 7.4 at 37°C. The pH values were selected to represent the pH's of blood (pH 7.4) and endosomes (pH 5.5–6.4) [40, 41]. The results showed that less than 10% of DOX was released at pH 7.4 in the first 4 h, and just over 30% of DOX was released after 72 h (Fig. 4c). At slight acidic pH (6.4) of early endosomes, the drug release increased: 12% at 4 h, and 40% at 72 h. At the lower pH (5.5) of late endosomes [41], a significantly higher amount of the drug was released in the same time period with nearly 15% of DOX released in the first 4 h, and over 55% in 72 h.

3.3. MR imaging

The MR relaxivity of NP-DOX was determined by MR imaging of nanoparticles dispersed in agarose gel (Fig. 5). The NP-DOX showed T_2 contrast enhancement under a T_2-weighed imaging sequence and r_2 relaxivity of 146 $mM^{-1}•s^{-1}$ (the slope of the relaxation vs. iron concentration curve). This r_2 relaxivity was similar to previously reported nanoparticle systems with a comparable iron oxide core diameter [16].

3.4. Dose-response results

To examine the cytotoxic effect of nanoparticles in drug-resistant cell populations, C6-ADR cells were treated with either free DOX or NP-DOX, and the viability of treated cells was determined by the Alamar blue assay at 24 and 72 h after treatment (Fig. 6). In this study, only drug-resistant cells were used because the difference in overcoming drug resistance between free drug and nanoparticle-carried drug could appear only in drug-resistant cells [42–44]. It should also be noted that free DOX could have a lower IC50 in non-drug resistant cells because these cells lack multidrug efflux pumps and thus are not suitable for the current investigation targeted at overcoming ABC transporter-mediated drug efflux. At the 24 h time point, NP-DOX showed a concentration of 0.846 ± 0.050 μg/mL that is required to induce cell death in half of the population (IC_{50}), comparable to free DOX (0.748 ± 0.146 μg/mL), with no significant statistical difference, indicating comparable cytotoxicity. At the 72 h time point, NP-DOX showed a significantly lower IC_{50} (0.386 ± 0.04 μg/mL) than free DOX (1.102 ± 0.105 μg/mL), indicating higher efficacy against C6-ADR. To verify that cytotoxicity was caused by DOX not by other nanoparticle components, we evaluated control nanoparticles that were coated with copolymer only (PBAE-C, without DOX). We found that the control nanoparticles did not cause any cytotoxicity up to 100 μg/mL of iron (Fig. S1, see Supplementary Information). This maximum tolerance iron dose equals to iron concentration of NP-DOX at 67.9 μg/mL DOX, well above the upper range of DOX (10 μg/mL) for the dose-response experiment.

3.5. Cellular internalization of nanoparticles

To study the mechanism behind the improved therapeutic efficacy against C6-ADR cells demonstrated by NP-DOX shown above, we compared the accumulation of NP-DOX and free DOX in C6-ADR cells. We first characterized the internalization of iron by C6-ADR cells using the Ferrozine assay to ensure that DOX was delivered by cellular internalization of NP-DOX, rather than passive diffusion of released DOX from extracellular space. NP-DOX showed significant amounts of internalization (2.24 ± 0.09 pg/cell) 4 hours after NP-DOX treatment (Fig. 7a). A decline in the intracellular iron concentration was observed at 24 hours after treatment (1.42 ± 0.15 pg/cell), which could be attributed to the cell divisions. The iron content per cell is decreased as the number of cells is increased.

Concurrently, intracellular concentration of DOX was determined (Fig. 7b) by UV analysis. Four hours after treatment, the intracellular concentration of DOX was comparable between free DOX treated (1.49 ± 0.05 pg/cell) and NP-DOX treated (1.54 ± 0.24 pg/cell) C6-ADR cells. However, at 24 h after treatment, the intracellular concentration of DOX in cells treated with NP-DOX (0.52 ± 0.06 pg/cell) was 4-fold higher than in cells treated with free DOX (0.13 ± 0.01 pg/cell).

The intracellular accumulation of free DOX and NP-DOX was further visualized by fluorescence microscopy (Fig. 8) after C6-ADR cells were treated with either DOX or NP-DOX for 4 h and fixed for another 20 h. Cells treated with free DOX had minimal fluorescence observed, while those treated with NP-DOX showed significant fluorescence signal in the perinuclear region of the cells. The internalization pathway of free DOX and NP-DOX were investigated by labeling endosomal compartments of cells with calcein

(green) after incubation with cells for 4h (Fig 9). The colocalization of DOX and calcein signals was clearly observed for cells treated with NP-DOX. For cells treated with free DOX, the DOX signal was partially colocalized with nucleus and partially localized in cytoplasma.

4. Discussion

The synthesis of PBAE-DOX is a single-step procedure where monomers are directly mixed with a minimum amount of solvent. The end product is easily separated by precipitation with organic solvents (such as ether, hexane) and purified by size-exclusion chromatography (SEC). Since DOX, PEG, and DA all contain primary amine groups, they can be directly incorporated into the backbone of PBAE (Fig. 1b). Thus, this method eliminates the need of multiple conjugation steps used in a conventional method where each component is individually attached to polymer coating and the amount of each component can be limited and difficult to control. The small difference between the feeding and loading of drug molecules (<7%, Fig. 3a) indicates high efficient conversion of free drug to conjugated drug during the polymerization reaction. Therefore, by altering the feeding ratio of monomers, the drug/polymer composition in the end product can be precisely controlled.

The drug loading efficiency and release kinetics are both important for the success of a drug delivery system. The drug loading of NP-DOX is directly correlated with the amount of drug in PBAE-DOX. This allows for precise control of the final component ratio of the nanoparticle coating by simply using PBAE-DOX with predetermined component ratios. High drug loading is preferable since it would reduce the dosage of pharmaceutically inactive ingredients, minimizing unintended toxicity and improving the safety profile of nanoparticle-based therapeutics. Systemic fast release kinetics can be detrimental to effective therapeutic treatment since premature drug release in the circulatory system could cause off-target accumulation resulting in unwanted toxicity. The strategy of incorporating drugs to carriers via polymerization has its advantage than loading drugs to carriers via non-covalent interaction in which it is impossible to determine the theoretical drug-loading ratio beforehand and drug-loading is generally lower than 9.5% achieved in this study [17, 21]. Furthermore, drug liberated before cellular internalization (i.e., extracellular drug release) would enter the target cells by passive diffusion similar to free drug, severely reducing the overall efficacy due to the MDR effects of target cells. Our drug release study showed that NP-DOX releases DOX at a fairly slow rate at physiological pH. The reasonable stability of ester bonds would allow sufficient time for NP-DOX to reach the tumor site and be internalized by tumor cells, without releasing DOX prematurely. At low pH, the release rate of DOX increases, suggesting that drug release would be greatly accelerated after NP-DOX are endocytosed by cancer cells where a lower pH environment in endosomes or lysosomes enhances the cleavage of ester bonds. Our study also suggests that a fraction of drug could not be released even after 72 h of incubation, possibly due to strong interactions with the surface of the iron oxide core or PBAE carrier polymer.

In vivo applications mandate that nanoparticle-based therapeutics should have a desirable range of hydrodynamic size and surface charge. Nanoparticles are required to be in a narrow size range to avoid elimination by kidneys (<10 nm) and minimizes liver and spleen uptake (>200 nm) [4]. Additionally, nanoparticles must maintain their stability in the presence of salts and biomacromolecules at elevated concentrations to prevent embolism and phagocytosis. The hydrodynamic sizes of NP-DOX are about 136 nm, and the zeta potential is near neutral at physiological pH. The stability of NP-DOX in culture media (Fig. 4b) can be attributed to the presence of PEG in the nanoparticle surface coating and near-neutral zeta potential. Not only are PEG molecules very hydrophilic, but they also form coiled conformations in aqueous solutions, providing excellent steric stabilization [20].

Additionally, the anti-fouling property of surface-bound PEG molecules can alleviate opsonization of serum protein, and thus, could reduce liver and macrophage uptake when used in vivo.

The ability to monitor drug delivery non-invasively and with high sensitivity is a desirable property of theranostic nanoparticles. The r_2 relaxivity of NP-DOX is similar to the previously reported nanoparticle system with a comparable iron oxide core diameter [16]. Since MRI is non-invasive and is not limited by the depth of the signal source, NP-DOX could be utilized for real-time drug delivery tracking and non-invasive treatment response assessment [5, 45, 46].

In drug-resistant cells like C6-ADR, intracellular free drug molecules can be removed from cytosol to extracellular space by ABC-mediated drug efflux [1]. This process greatly lowers the effective intracellular drug concentration and reduces the efficacy of free drug in drug-resistant cells. Conversely, nanoparticle-based drug delivery vehicles could circumvent ABC-mediated drug efflux mechanism by maintaining a sustained intracellular drug concentration that is sufficient to damage target organelles. This study showed superiority of NP-DOX over free DOX in overcoming the efflux by C6-ADR cells. At 24 hrs after treatment, the IC50 of free DOX and NP-DOX for C6-ADR cells are similar, likely due to the slow release kinetics of NP-DOX. Therefore, significant cell kill over what can be achieved by free DOX was not observed. Conversely, after 72 hrs, the nanoparticles-drug conjugate achieved significantly better efficacy (65% reduction of IC50) than the free drug in drug-resistant cells (Fig. 6). This suggests that the drug release profile of NP-DOX is able to maintain a higher intracellular DOX concentration for improved and prolonged cell kill.

To reveal the mechanism for improved cell kill imparted by NP-DOX, the intracellular nanoparticle and DOX concentrations were monitored over time. Ferrozine assay results indicated that an initial uptake of free DOX by C6-ADR cells is similar to NP-DOX. However, the intracellular DOX concentration of cells treated with free DOX dropped precipitously (91% decrease) by 24 h after initial exposure, significantly lower than in cells treated with NP-DOX. The results suggest that ABC-transporters expressed in C6-ADR cells effectively reduced intracellular free DOX, while NP-DOX was able to maintain a substantial total DOX concentration (cleaved and conjugated DOX) after 24 h (about one third of the value of 4 h). Therefore, ABC transporter mediated MDR was mitigated by nanoparticle internalization and controlled release of drug. This prolonged release of drug likely accounts for the observed improvement in cell kill after 72 hrs. Visualization of C6-ADR cells by fluorescence microscopy further confirmed that NP-DOX aided in mitigating MDR in cancer cells. Since DOX is a small-molecule drug, free DOX can readily diffused into cells. Free DOX showed significant fluorescence at cell nuclei and near cell membrane right after treatment (Fig. 9), indicating rapid internalization of DOX and possible removal by ABC-mediated drug-efflux. Minimal fluorescence was observed 24 h after treatment (Fig. 8), indicating that free DOX was effectively removed by ABC-mediated drug-efflux. On the other hand, NP-DOX was much larger in size, and entered endosomes of cells by endocytosis, as shown in Fig. 9. Intracellular DOX signal was observed in the perinuclear region after 24 h (Fig. 8), suggesting a substantial amount of intracellular drug present. Sustained release of DOX from NP-DOX encapsulated by endosomes would result in higher cytotoxicity at 72 h.

In summary, we have introduced a simple synthesis method to prepare theranostic nanoparticles for delivery of cancer chemotherapeutics and MR imaging. The nanoparticle contains a superparamagnetic iron oxide core that exhibits T_2 contrast enhancement with a hydrophilic and biodegradable PBAE polymer as coating. This nanoparticle system offers a platform based on a simple and highly controllable synthesis scheme that can be tailored to

incorporate various therapeutic drugs, and adopt various drug release mechanisms such as reducing, enzymatic, or photolytic environments. The synthesis scheme is expected to dramatically improve the reproducibility of a nanoparticle formulation, and is easy and economical to scale up for mass production.

Supplementary Material

Refer to Web version on PubMed Central for supplementary material.

Acknowledgments

This work is supported in part by NIH grants R01CA134213 and R01EB006043. C.F. acknowledges the support through an NCI/NSF IGERT fellowship. O.V. F.M.K. and Z.S. acknowledge the support through an NIH/NCI training grant (T32CA138312). T.W. acknowledges financial support through Department of Neurological Surgery of the Fourth Affiliated Hospital of China Medical University. We acknowledge the use of resources at the Diagnostic Imaging Sciences Center and Center for Nanotechnology at the University of Washington. Lab assistance from Yong-Chan Cho is also acknowledged.

Abbreviations

ABC	ATP-binding cassette
DA	dopamine
DOX	doxorubicin
MDR	multidrug resistance
MRI	magnetic resonance imaging
PEG	poly (ethylene glycol)
NP-DOX	DOX-loaded nanoparticles
PBAE	poly (beta-amino ester)
SPIONs	superparamagnetic iron oxide nanoparticles

References

1. Gottesman MM, Fojo T, Bates SE. Multidrug resistance in cancer: role of ATP-dependent transporters. Nat Rev Cancer. 2002; 2:48–58. [PubMed: 11902585]
2. Szakacs G, Paterson JK, Ludwig JA, Booth-Genthe C, Gottesman MM. Targeting multidrug resistance in cancer. Nat Rev Drug Discov. 2006; 5:219–234. [PubMed: 16518375]
3. Peer D, Karp JM, Hong S, Farokhzad OC, Margalit R, Langer R. Nanocarriers as an emerging platform for cancer therapy. Nature Nanotech. 2007; 2:751–760.
4. Petros RA, Desimone JM. Strategies in the design of nanoparticles for therapeutic applications. Nat Rev Drug Discov. 2010; 9:615–627. [PubMed: 20616808]
5. Fang C, Zhang M. Nanoparticle-based theragnostics: Integrating diagnostic and therapeutic potentials in nanomedicine. J Control Release. 2010; 146:2–5. [PubMed: 20493220]
6. Lammers T, Kiessling F, Hennink WE, Storm G. Nanotheranostics and image-guided drug delivery: current concepts and future directions. Mol Pharm. 2010; 7:1899–1912. [PubMed: 20822168]
7. Lammers T, Aime S, Hennink WE, Storm G, Kiessling F. Theranostic nanomedicine. Accounts of chemical research. 2011; 44:1029–1038. [PubMed: 21545096]
8. Koo H, Huh MS, Sun IC, Yuk SH, Choi K, Kim K, Kwon IC. In vivo targeted delivery of nanoparticles for theranosis. Accounts of chemical research. 2011; 44:1018–1028. [PubMed: 21851104]
9. Fang C, Bhattarai N, Sun C, Zhang M. Functionalized nanoparticles with long-term stability in biological media. Small. 2009; 5:1637–1641. [PubMed: 19334014]

10. Sun C, Du K, Fang C, Bhattarai N, Veiseh O, Kievit F, Stephen Z, Lee D, Ellenbogen RG, Ratner B, Zhang M. PEG-mediated synthesis of highly dispersive multifunctional superparamagnetic nanoparticles: their physicochemical properties and function in vivo. ACS Nano. 2010; 4:2402–2410. [PubMed: 20232826]
11. Kievit FM, Veiseh O, Fang C, Bhattarai N, Lee D, Ellenbogen RG, Zhang M. Chlorotoxin labeled magnetic nanovectors for targeted gene delivery to glioma. ACS Nano. 2010; 4:4587–4594. [PubMed: 20731441]
12. Kievit FM, Zhang M. Surface Engineering of Iron Oxide Nanoparticles for Targeted Cancer Therapy. Acc Chem Res. 2011 In press.
13. Veiseh O, Gunn JW, Zhang M. Design and fabrication of magnetic nanoparticles for targeted drug delivery and imaging. Adv Drug Deliv Rev. 2010; 62:284–304. [PubMed: 19909778]
14. Xie J, Liu G, Eden HS, Ai H, Chen X. Surface-Engineered Magnetic Nanoparticle Platforms for Cancer Imaging and Therapy. Acc Chem Res. 2011 In press.
15. Veiseh O, Kievit FM, Fang C, Mu N, Jana S, Leung MC, Mok H, Ellenbogen RG, Park JO, Zhang M. Chlorotoxin bound magnetic nanovector tailored for cancer cell targeting, imaging, and siRNA delivery. biomaterials. 2010; 31:8032–8042. [PubMed: 20673683]
16. Sun C, Du K, Fang C, Bhattarai N, Veiseh O, Kievit F, Stephen Z, Lee D, Ellenbogen RG, Ratner B, Zhang M. PEG-Mediated Synthesis of Highly Dispersive Multifunctional Superparamagnetic Nanoparticles: Their Physicochemical Properties and Function In Vivo. ACS Nano. 2010
17. Guthi JS, Yang S-G, Huang G, Li S, Khemtong C, Kessinger CW, Peyton M, Minna JD, Brown KC, Gao J. MRI-visible micellar nanomedicine for targeted drug delivery to lung cancer cells. Mol Pharm. 2010; 7:32–40. [PubMed: 19708690]
18. Zou P, Yu Y, Wang YA, Zhong Y, Welton A, Galbán C, Wang S, Sun D. Superparamagnetic iron oxide nanotheranostics for targeted cancer cell imaging and pH-dependent intracellular drug release. Mol Pharm. 2010; 7:1974–1984. [PubMed: 20845930]
19. Kievit FM, Veiseh O, Bhattarai N, Fang C, Gunn JW, Lee D, Ellenbogen RG, Olson JM, Zhang M. PEI-PEG-Chitosan-Copolymer-Coated Iron Oxide Nanoparticles for Safe Gene Delivery: Synthesis, Complexation, and Transfection. Adv Funct Mater. 2009; 19:2244–2251. [PubMed: 20160995]
20. Fang C, Bhattarai N, Sun C, Zhang M. Functionalized nanoparticles with long-term stability in biological media. Small. 2009; 5:1637–1641. [PubMed: 19334014]
21. Jain TK, Morales MA, Sahoo SK, Leslie-Pelecky DL, Labhasetwar V. Iron oxide nanoparticles for sustained delivery of anticancer agents. Mol Pharm. 2005; 2:194–205. [PubMed: 15934780]
22. Kievit FM, Wang FY, Fang C, Mok H, Wang K, Silber JR, Ellenbogen RG, Zhang M. Doxorubicin loaded iron oxide nanoparticles overcome multidrug resistance in cancer in vitro. J Control Release. 2010
23. Kohler N, Sun C, Fichtenholtz A, Gunn J, Fang C, Zhang M. Methotrexate-immobilized poly(ethylene glycol) magnetic nanoparticles for MR imaging and drug delivery. Small. 2006; 2:785–792. [PubMed: 17193123]
24. Kohler N, Sun C, Wang J, Zhang M. Methotrexate-modified superparamagnetic nanoparticles and their intracellular uptake into human cancer cells. Langmuir. 2005; 21:8858–8864. [PubMed: 16142971]
25. Lee Y, Lee H, Kim YB, Kim J, Hyeon T, Park H, Messersmith PB, Park TG. Bioinspired Surface Immobilization of Hyaluronic Acid on Monodisperse Magnetite Nanocrystals for Targeted Cancer Imaging. Adv Mater. 2008; 20:4154–4157. [PubMed: 19606262]
26. Lai JR, Chang YW, Yen HC, Yuan NY, Liao MY, Hsu CY, Tsai JL, Lai PS. Multifunctional doxorubicin/superparamagnetic iron oxide-encapsulated Pluronic F127 micelles used for chemotherapy/magnetic resonance imaging. J. Appl. Phys. 2010; 107:3.
27. Yang J, Lee CH, Ko HJ, Suh JS, Yoon HG, Lee K, Huh YM, Haam S. Multifunctional magneto-polymeric nanohybrids for targeted detection and synergistic therapeutic effects on breast cancer. Angew Chem Int Ed Engl. 2007; 46:8836–8839. [PubMed: 17943947]
28. Sanson C, Diou O, Thevenot J, Ibarboure E, Soum A, Brulet A, Miraux S, Thiaudiere E, Tan S, Brisson A, Dupuis V, Sandre O, Lecommandoux S. Doxorubicin Loaded Magnetic

Polymersomes: Theranostic Nanocarriers for MR Imaging and Magneto-Chemotherapy. ACS Nano. 2011; 5:1122–1140. [PubMed: 21218795]

29. Abdalla MO, Karna P, Sajja HK, Mao H, Yates C, Turner T, Aneja R. Enhanced noscapine delivery using uPAR-targeted optical-MR imaging trackable nanoparticles for prostate cancer therapy. J. Control. Release. 2011; 149:314–322. [PubMed: 21047537]
30. Andrew Mackay J, Chen M, McDaniel J, Liu W, Simnick A, Chilkoti A. Self-assembling chimeric polypeptide-doxorubicin conjugate nanoparticles that abolish tumours after a single injection. Nat Mater. 2009
31. Anderson DG, Lynn DM, Langer R. Semi-Automated Synthesis and Screening of a Large Library of Degradable Cationic Polymers for Gene Delivery. Angew Chem Int Ed. 2003; 42:3153–3158.
32. Huang Y-H, Zugates GT, Peng W, Holtz D, Dunton C, Green JJ, Hossain N, Chernick MR, Padera RF, Langer R, Anderson DG, Sawicki JA. Nanoparticle-delivered suicide gene therapy effectively reduces ovarian tumor burden in mice. Cancer Res. 2009; 69:6184–6191. [PubMed: 19643734]
33. Zugates GT, Anderson DG, Little SR, Lawhorn IEB, Langer R. Synthesis of poly(beta-amino ester)s with thiol-reactive side chains for DNA delivery. J Am Chem Soc. 2006; 128:12726–12734. [PubMed: 17002366]
34. Shen Y, Tang H, Zhan Y, Van Kirk EA, Murdoch WJ. Degradable poly(beta-amino ester) nanoparticles for cancer cytoplasmic drug delivery. Nanomedicine. 2009; 5:192–201. [PubMed: 19223244]
35. Wu XL, Kim JH, Koo H, Bae SM, Shin H, Kim MS, Lee BH, Park RW, Kim IS, Choi K, Kwon IC, Kim K, Lee DS. Tumor-targeting peptide conjugated pH-responsive micelles as a potential drug carrier for cancer therapy. Bioconjug Chem. 2010; 21:208–213. [PubMed: 20073455]
36. Nitiss JL. Targeting DNA topoisomerase II in cancer chemotherapy. Nat Rev Cancer. 2009; 9:338–350. [PubMed: 19377506]
37. N.C. Institute. NCI Thesaurus. National Cancer Institute; 2010.
38. Sun S, Zeng H, Robinson DB, Raoux S, Rice PM, Wang SX, Li G. Monodisperse MFe2O4 (M = Fe, Co, Mn) nanoparticles. J Am Chem Soc. 2004; 126:273–279. [PubMed: 14709092]
39. Fang C, Veiseh O, Kievit F, Bhattarai N, Wang F, Stephen Z, Li C, Lee D, Ellenbogen RG, Zhang M. Functionalization of iron oxide magnetic nanoparticles with targeting ligands: their physicochemical properties and in vivo behavior. Nanomedicine (Lond). 2004; 5:1357–1369. [PubMed: 21128719]
40. Guo M, Yan Y, Liu X, Yan H, Liu K, Zhang H, Cao Y. Multilayer nanoparticles with a magnetite core and a polycation inner shell as pH-responsive carriers for drug delivery. Nanoscale. 2010; 2:434–441. [PubMed: 20644829]
41. Pack DW, Hoffman AS, Pun S, Stayton PS. Design and development of polymers for gene delivery. Nature Reviews Drug Discovery. 2005; 4:581–593.
42. Kievit FM, Wang FY, Fang C, Mok H, Wang K, Silber JR, Ellenbogen RG, Zhang M. Doxorubicin loaded iron oxide nanoparticles overcome multidrug resistance in cancer in vitro. J Control Release. 2011
43. Andrew Mackay J, Chen M, McDaniel J, Liu W, Simnick A, Chilkoti A. Self-assembling chimeric polypeptide-doxorubicin conjugate nanoparticles that abolish tumours after a single injection. Nature Materials. 2009
44. Chaudhuri P, Paraskar A, Soni S, Mashelkar R, Sengupta S. Fullerenol-Cytotoxic Conjugates for Cancer Chemotherapy. ACS Nano. 2009
45. Shubayev VI, Pisanic TR 2nd, Jin S. Magnetic nanoparticles for theragnostics. Adv Drug Deliv Rev. 2009:467–477. [PubMed: 19389434]
46. Liu HL, Hua MY, Yang HW, Huang CY, Chu PC, Wu JS, Tseng IC, Wang JJ, Yen TC, Chen PY, Wei KC. Magnetic resonance monitoring of focused ultrasound/magnetic nanoparticle targeting delivery of therapeutic agents to the brain. Proc Natl Acad Sci U S A. 2010; 107:15205–15210. [PubMed: 20696897]

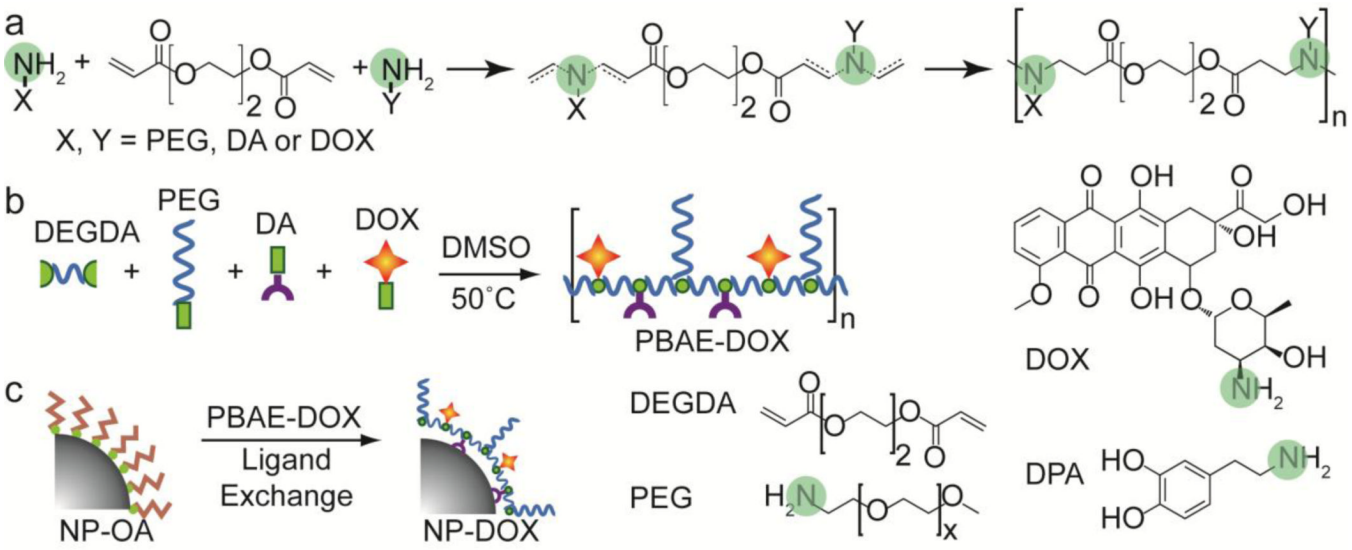

Fig. 1.

Schematic illustration of PBAE synthesis and nanoparticle surface modification. (a) General scheme for synthesis of PBAE copolymer through Michael addition reaction. Amine groups are highlighted in green. (b) Formation of PBAE-DOX through reaction between DEGDA, PEG, DA and DOX. Note: this illustration does not reflect the exact sequence and ratio of each component. (c) Formation of NP-DOX via ligand-exchange reaction.

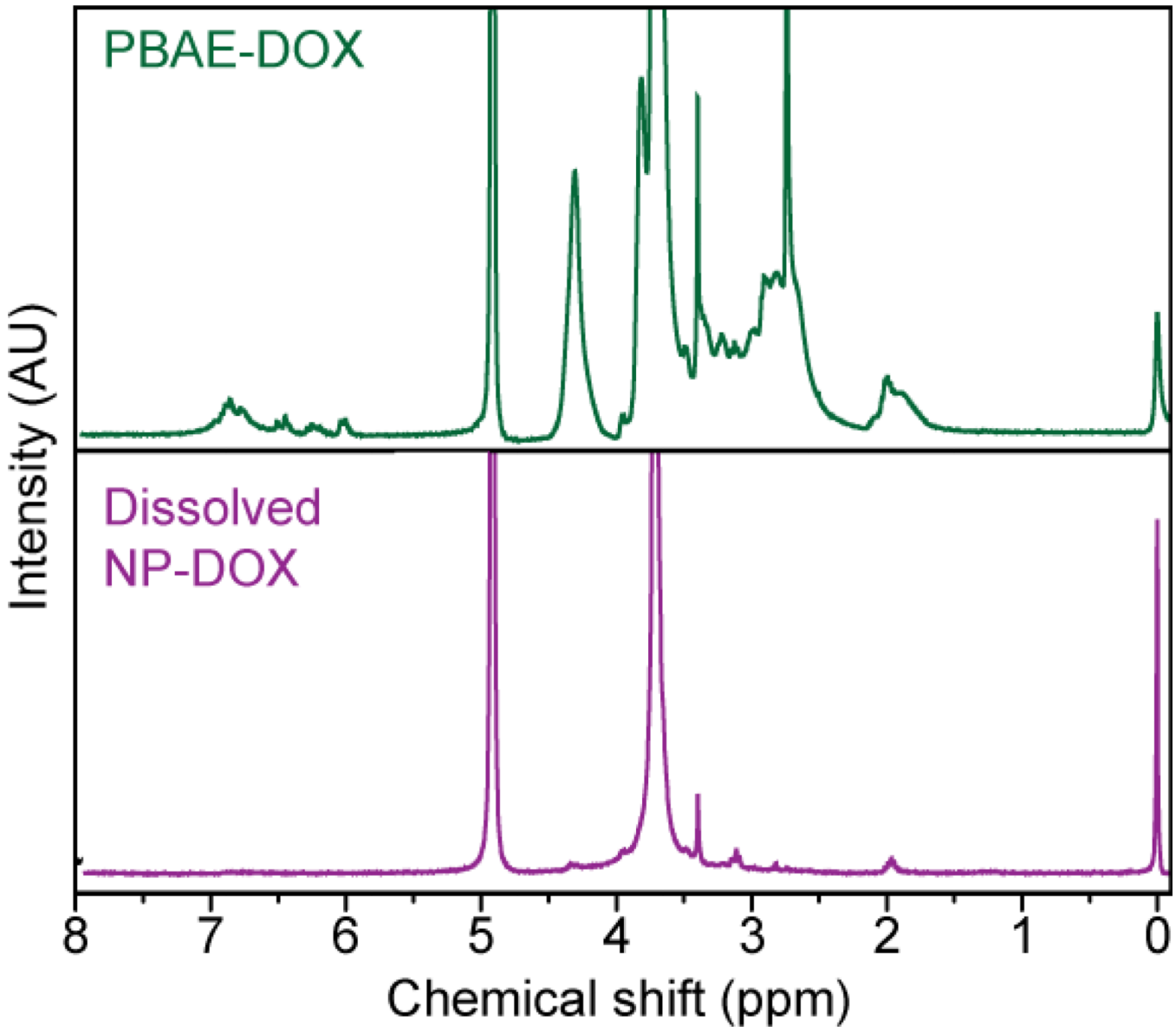

Fig. 2.
NMR spectra of PBAE-DOX (upper panel) and NP-DOX dissolved in DCl/D_2O (lower panel).

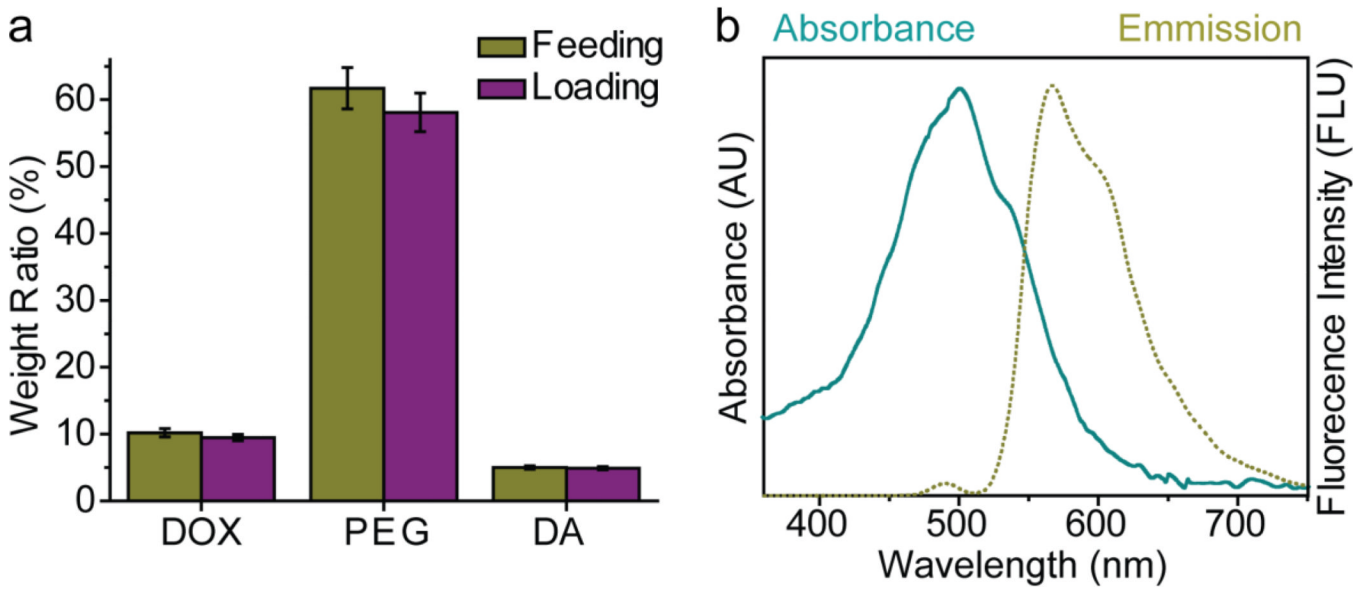

Fig. 3.

Properties of PBAE polymers. (a) Comparison chart of PEG, DOX, and DA feeding and loading ratios in PBAE polymer. Here, the feeding and loading ratios refer to the weight ratios of each component in the reactants and product (PBAE-DOX), respectively. (b) Absorbance spectra of DOX in PBAE-DOX.

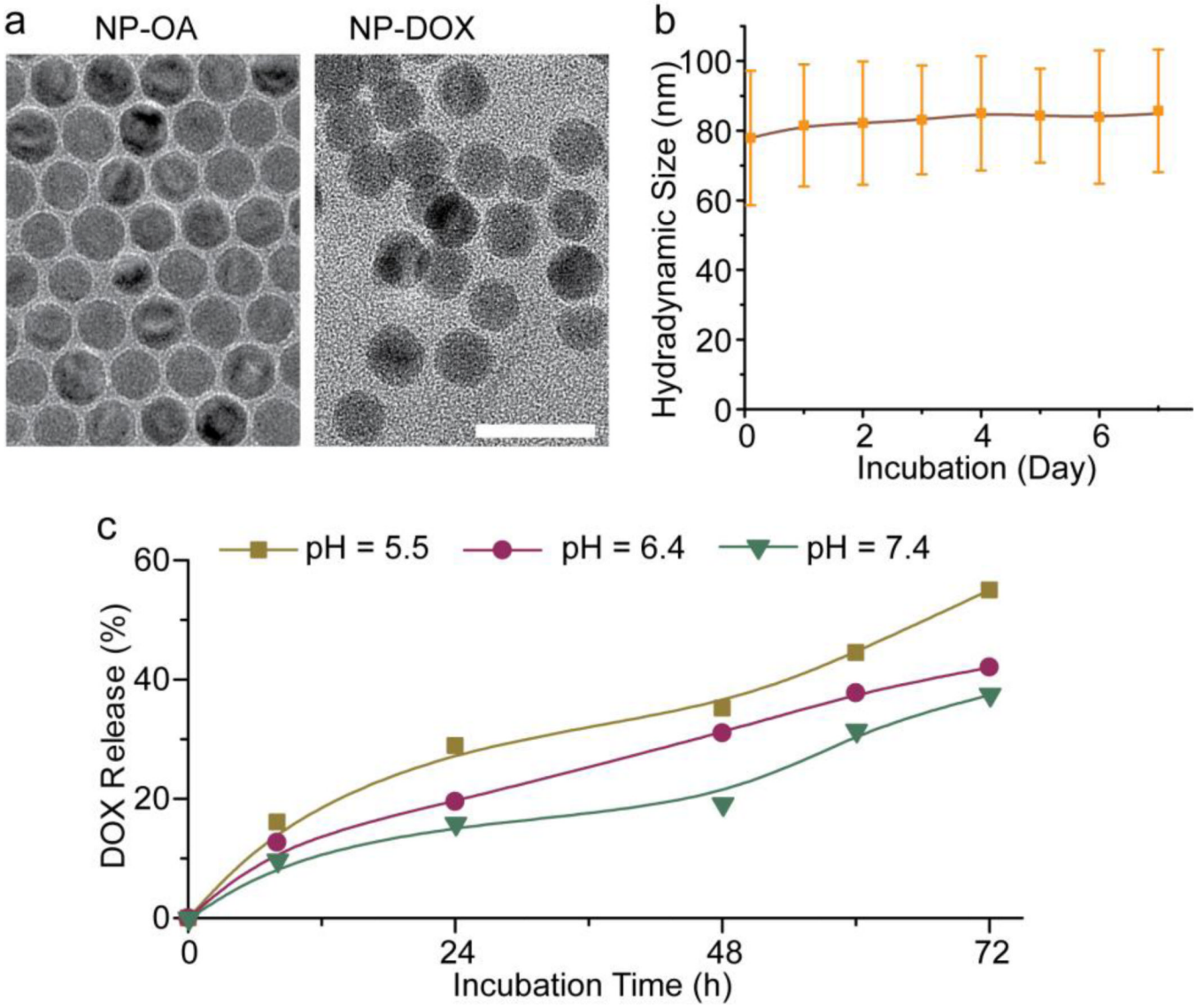

Fig. 4.

Physicochemical Properties of NP-DOX. (a) TEM images of NP-OA and NP-DOX. The scale bar: 20 nm. (b) Hydrodynamic size of NP-DOX in cell culture media (DMEM with 10% FBS) as a function of time. (c) Drug release profiles of DOX from NP-DOX in solutions of pH 5.5, pH 6.4 and pH 7.4 at 37°C.

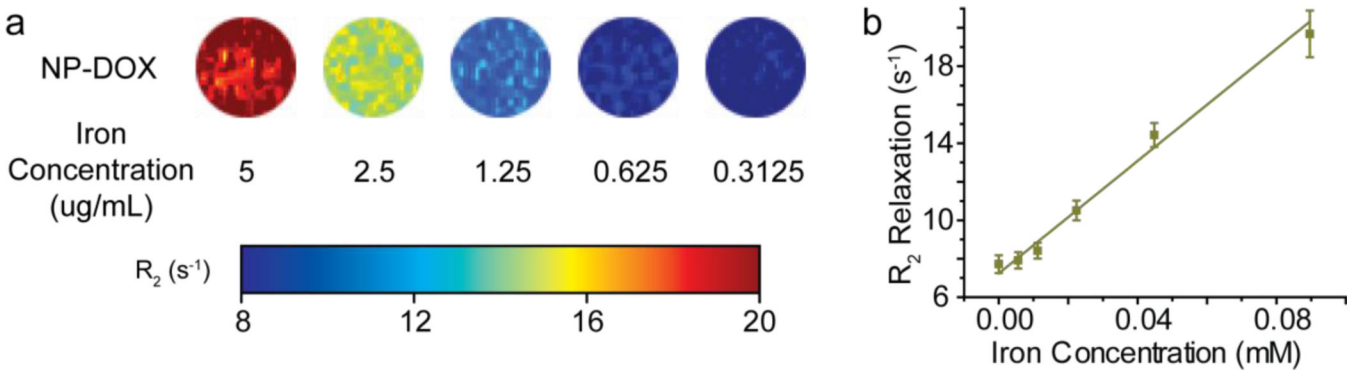

Fig. 5.

Magnetic properties of NP-DOX. (a) MR phantom images of NP-DOX of different iron concentrations. (b) R_2 magnetic relaxation of NP-DOX as a function of iron concentration.

a

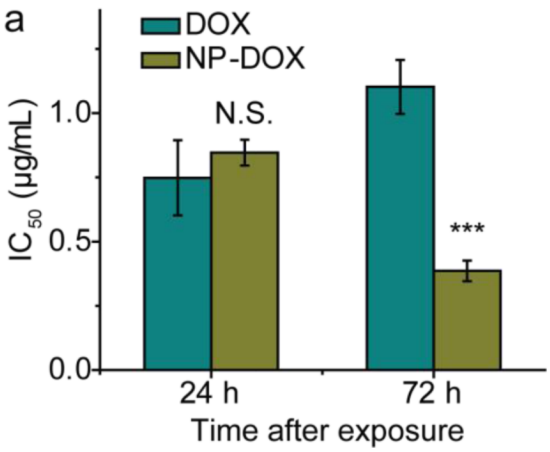

b

Name	24 h	72 h
DOX	0.748 ± 0.146	1.102 ± 0.105
NP-DOX	0.846 ± 0.050	0.386 ± 0.040
p Value	> 0.05	< 0.001

Fig. 6.

IC_{50} values (in μg/mL) of free DOX and NP-DOX. (a) Graphic presentation of DOX and NP-DOX at 24 h and 72 h after treatment of C6-ADR cells. (b) Table of IC_{50} values of free DOX and NP-DOX at 24 h and 72 h after treatment of C6-ADR cells. p values were determined by Student's *t*-test. N.S. indicates no significance, *** indicates $P < 0.001$.

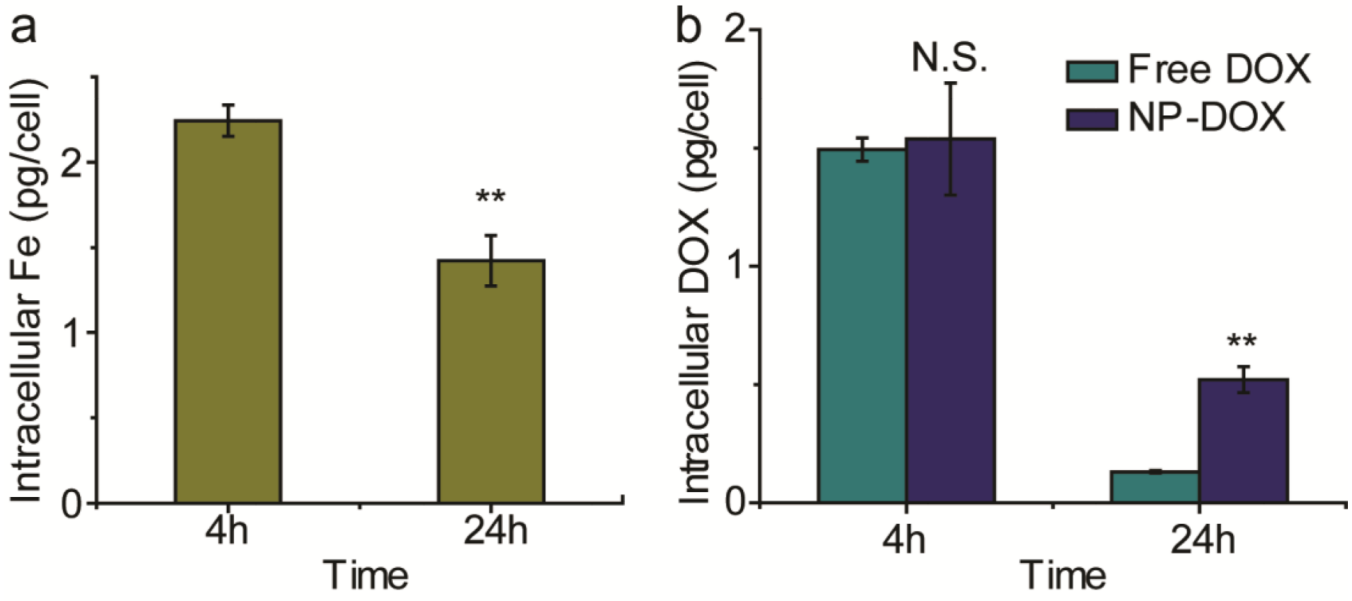

Fig. 7.

Cellular internalization studies for free DOX and NP-DOX. (a) Intracellular iron quantification of C6-ADR cells at 4 h and 24 h after initial exposure to NP-DOX. (b) Intracellular DOX quantification of C6-ADR cells at 4 h and 24 h after initial exposure to NP-DOX or free DOX. N.S. indicates no significance, ** indicates $p < 0.01$, as determined by Student's *t*-test.

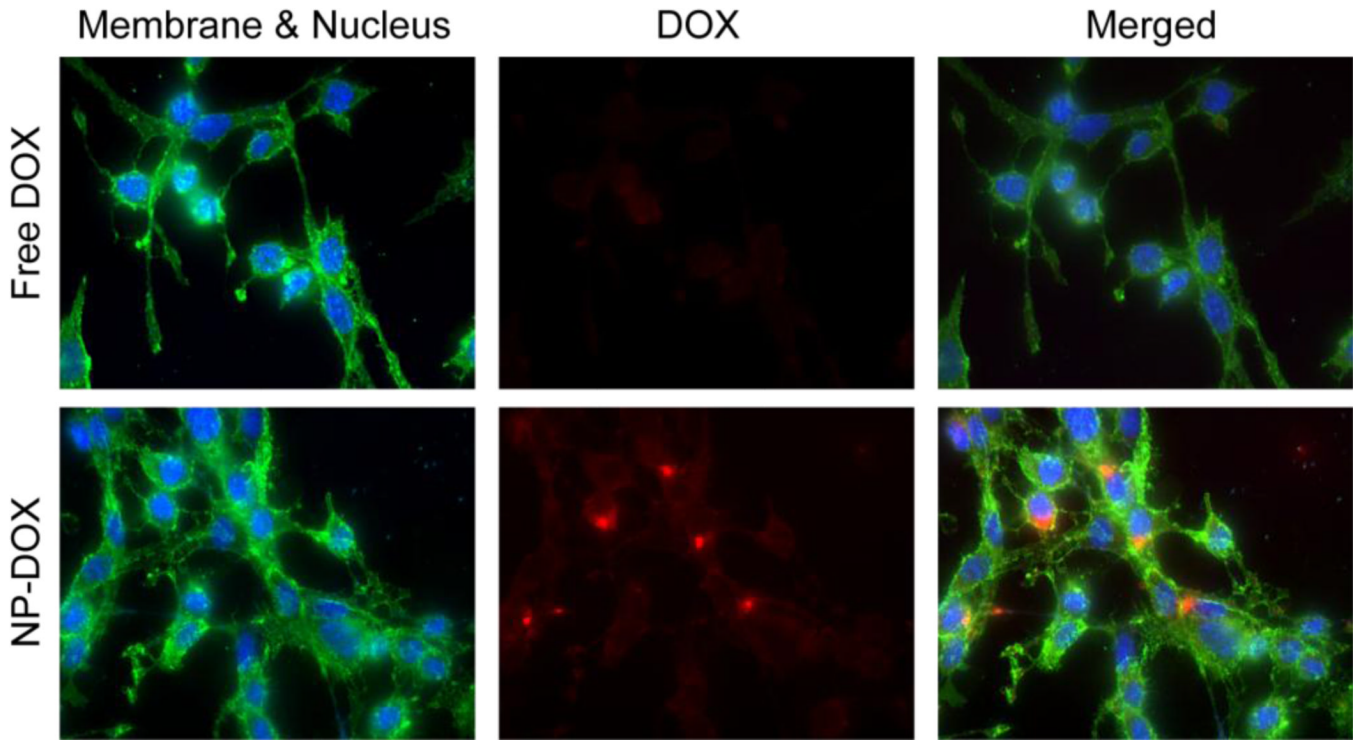

Fig. 8.

Fluorescence imaging of C6-ADR cells 24 h after the initial incubation with free DOX or NP-DOX, where cell nuclei were shown in blue, the DOX fluorescence in red, and cell membranes in green (WGA-AF488).

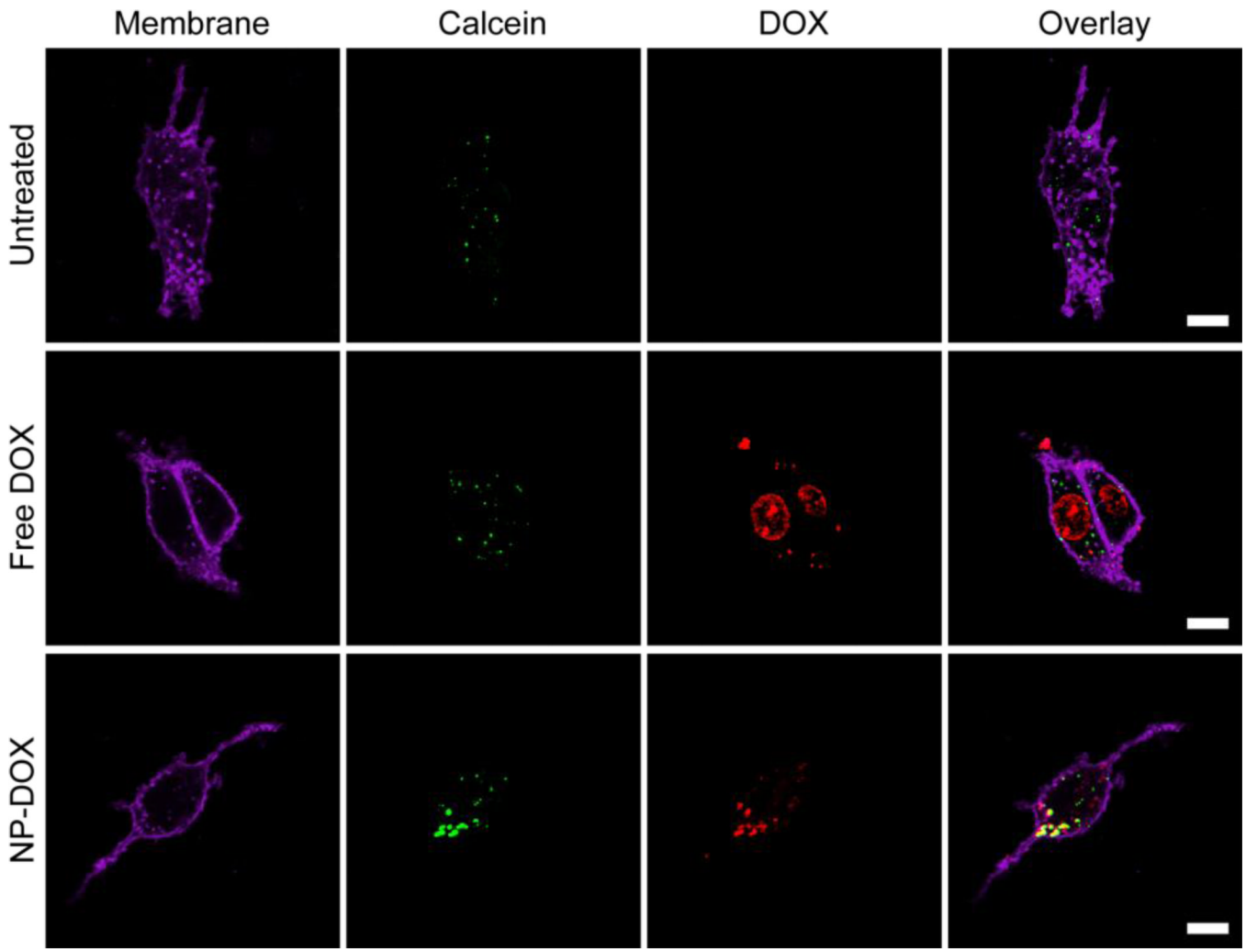

Fig. 9.

Confocal images of C6-ADR cells 4 h after incubation with either NP-DOX or free DOX. Endosomal compartments of cells were labeled with calcein (green, column 2), the DOX fluorescence was shown in red (column 3), and cell membranes in purple (WGA-AF647, column 1). The overlap of DOX and calcein signals, which yields yellow coloration (column 4), suggests that DOX resides in endosomal compartments. The scale bar corresponds to 10 μm.

Table 1

Physicochemical properties of PBAE polymers

Name	Molar ratio (DEGBA: PEG: DA: DOX)	Drug loading (%)	PEG content (%)	Yield (%)
PBAE-DOX	50:19:19:12	9.5	58.1	42
PBAE-C	50:25:25:0	0.0	65.1	69

Table 2

Physicochemical properties of NP-DOX.

Name	Size in PBS (nm)	Zeta potential at pH 7.4 (mV)	Polymer loading (μg/mg Fe)	Drug loading (μg/mg Fe)
NP-DOX	80.5 ± 38.3[a]	−0.3 ± 3.9[b]	7147 ± 651[c]	679 ± 40[c]

[a] PDI width;

[b] Zeta potential deviation;

[c] Standard deviation